Stem Cell Reports
Article

ISSCR

OPEN ACCESS

A Single Radioprotective Dose of Prostaglandin E_2 Blocks Irradiation-Induced Apoptotic Signaling and Early Cycling of Hematopoietic Stem Cells

Andrea M. Patterson,[1,5] Liqiong Liu,[1,5] Carol H. Sampson,[2] P. Artur Plett,[2] Hongge Li,[1] Pratibha Singh,[1] Khalid S. Mohammad,[3] Jonathan Hoggatt,[4] Maegan L. Capitano,[1] Christie M. Orschell,[2,6,*] and Louis M. Pelus[1,2,6,*]

[1]Department of Microbiology & Immunology, Indiana University School of Medicine, Indianapolis, IN, USA
[2]Department of Medicine/Hematology Oncology, Indiana University School of Medicine, Indianapolis, IN, USA
[3]Department of Medicine/Endocrinology, Indiana University School of Medicine, Indianapolis, IN, USA
[4]Center for Cancer Research and Center for Transplantation Sciences, Massachusetts General Hospital, Harvard Medical School, Harvard Stem Cell Institute, Boston, MA, USA
[5]Co-first author
[6]Co-senior author
*Correspondence: corschel@iupui.edu (C.M.O.), lpelus@iupui.edu (L.M.P.)
https://doi.org/10.1016/j.stemcr.2020.07.004

SUMMARY

Ionizing radiation exposure results in acute and delayed bone marrow suppression. Treatment of mice with 16,16-dimethyl prostaglandin E_2 ($dmPGE_2$) prior to lethal ionizing radiation (IR) facilitates survival, but the cellular and molecular mechanisms are unclear. In this study we show that $dmPGE_2$ attenuates loss and enhances recovery of bone marrow cellularity, corresponding to a less severe hematopoietic stem cell nadir, and significantly preserves long-term repopulation capacity and progenitor cell function. Mechanistically, $dmPGE_2$ suppressed hematopoietic stem cell (HSC) proliferation through 24 h post IR, which correlated with fewer DNA double-strand breaks and attenuation of apoptosis, mitochondrial compromise, oxidative stress, and senescence. RNA sequencing of HSCs at 1 h and 24 h post IR identified a predominant interference with IR-induced p53-downstream gene expression at 1 h, and confirmed the suppression of IR-induced cell-cycle genes at 24 h. These data identify mechanisms of $dmPGE_2$ radioprotection and its potential role as a medical countermeasure against radiation exposure.

INTRODUCTION

Billions of new blood cells are required daily to maintain homeostasis and respond to stressors such as infection, bleeding, or cell damage. The hematopoietic system is extremely sensitive to ionizing radiation (IR) (Till and McCulloch, 1964), which results in dose-dependent bone marrow suppression known as the hematopoietic acute radiation syndrome (H-ARS), characterized by pancytopenia and possible death from hemorrhage or infection (Dainiak et al., 2003). These life-threatening effects result from damage to DNA and other components of hematopoietic stem cells (HSCs) and hematopoietic progenitor cells (HPCs) causing cell death or functional compromise (Shao et al., 2014).

Prostaglandin E_2 is a pleiotropic lipid with effects on multiple organ systems, including normal and stressed hematopoiesis (Hoggatt and Pelus, 2010; Pelus and Hoggatt, 2011). When administered prior to IR, E prostaglandins including 16,16-dimethyl prostaglandin E_2 ($dmPGE_2$), can improve survival (Steel et al., 1988; Walden et al., 1987), reduce intestinal stem cell and crypt damage (Hanson and Ainsworth, 1985; Hanson and Thomas, 1983), protect spermatogenesis (van Buul et al., 1999), and prevent alopecia (Hanson et al., 1992). Protection of the multipotent progenitor cell CFU-S (colony-forming unit—spleen) was also demonstrated (Hanson and Ainsworth, 1985; Walden et al., 1987). More recently, we and others demonstrated that $dmPGE_2$ can mitigate the effects of lethal IR on hematopoiesis (Hoggatt et al., 2013b; Porter et al., 2013). However, mechanisms whereby PGE_2 protects hematopoiesis or mitigates IR-induced damage are unknown.

In this study, we performed phenotypic and functional analyses of primitive hematopoietic cells from mice early after lethal-dose IR, and utilized RNA sequencing (RNA-seq) to identify critical pathways of IR-induced damage and radioprotection triggered by $dmPGE_2$ in HSCs.

RESULTS

$dmPGE_2$ Protects Hematopoiesis from Lethal IR

Using a model of H-ARS in which hematopoietic effects are responsible for mortality (Plett et al., 2012), we confirmed radioprotection by $dmPGE_2$. Single administration of $dmPGE_2$ 30 min prior to total body IR protected 100% of mice from a lethal dose of 8.53 Gy (Figure 1A). Given the single dose and short half-life of $dmPGE_2$, we hypothesized that its critical radioprotective effects are manifested early after IR before the onset of morbidity and mortality (~day 10), and evaluated bone marrow cells at 1 h, 24 h, 72 h, and 9 days post IR in mice pretreated with $dmPGE_2$

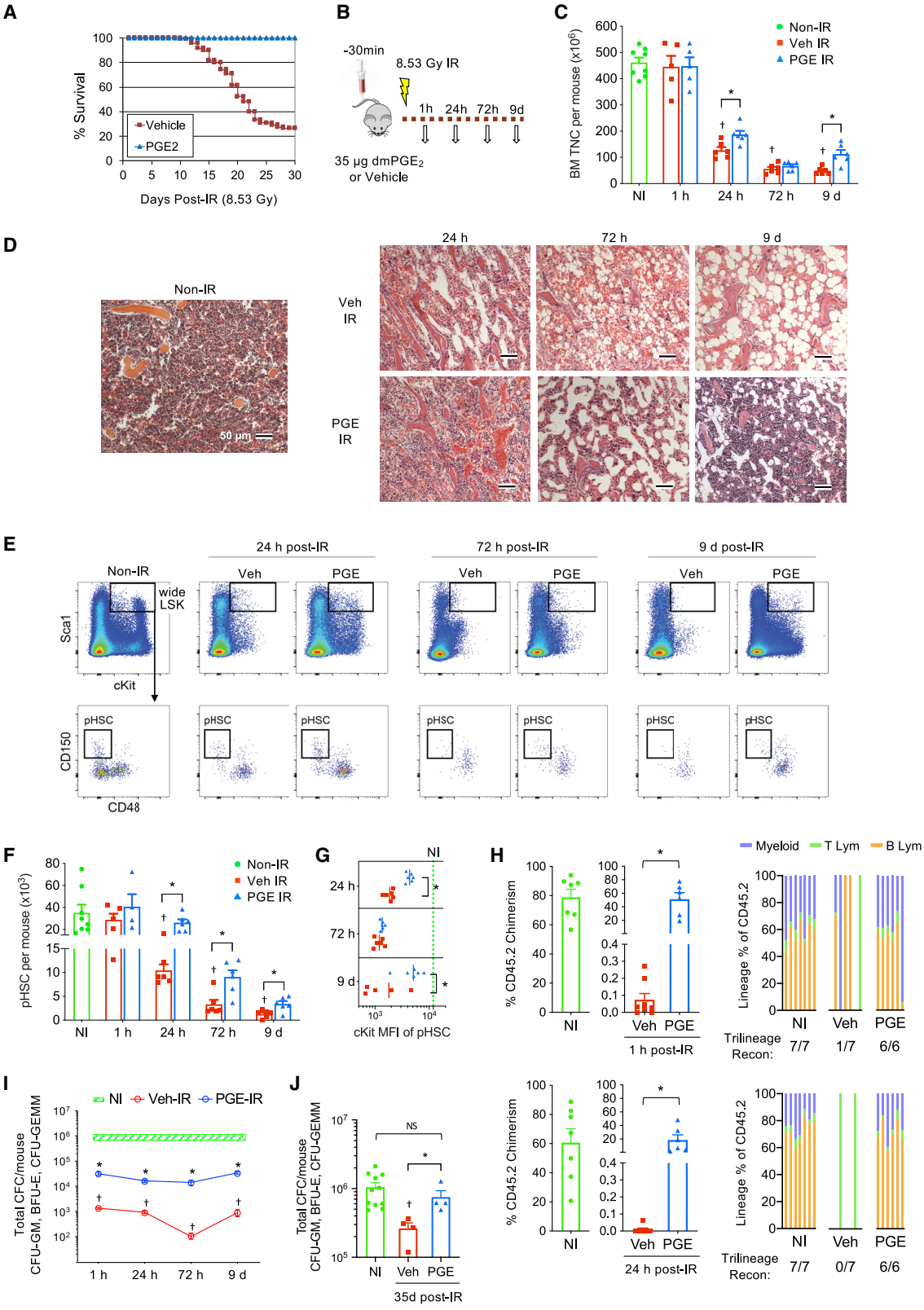

(legend on next page)

or vehicle (Figure 1B). IR produced a rapid and progressive decline in total nucleated cells (TNCs) that extended through 9 days post IR in the vehicle group, whereas TNCs declined less rapidly and began to rebound by day 9 in $dmPGE_2$-treated mice (Figure 1C).

Histology further illustrated attenuation of hematopoietic cell loss at 24 h and 72 h post IR by $dmPGE_2$, with marrow volume rebounding by 9 days to ~70% of total tissue volume compared with 5% in the vehicle group (Figures 1D, S1A, and S1B). The marrow cavity of vehicle-treated mice displayed adipocyte accumulation throughout the time course and the presence of red blood cell infiltration, which suggests potential loss of sinusoidal integrity. In contrast, little or no adipocytes or red blood cells outside sinusoids were apparent at any time point in mice treated with $dmPGE_2$ (Figures 1D and S1A). The number of endosteal-lining osteolineage cells was unchanged (Figure S1C).

Effects of IR and $dmPGE_2$ on HSCs and HPCs

Standard flow-cytometric analysis of HSCs and HPCs becomes obscured post IR due to loss of surface c-Kit (Simonnet et al., 2009). To determine a reliable gating strategy, we subjected Fgd5 mice with HSC-specific green fluorescence (Gazit et al., 2014) to IR to track hematopoietic marker expression in HSCs (Figure S2). At steady state, HSCs are defined within the lineage$^-$, Sca-1$^+$, c-Kit$^+$ (LSK) population by SLAM family markers as CD150$^+$CD48$^-$ (SLAM-LSK) (Oguro et al., 2013). Green fluorescent HSCs were detectable 24 h and 72 h post IR with a progressive decline in surface c-Kit and increased Sca-1 as described by Simonnet et al. (2009). However, SLAM markers could isolate HSCs to equivalent purity without c-Kit at steady state (Kiel et al., 2005) and after IR (Figure S2). Thus, we adopted a "wide LSK" gating strategy to encompass c-Kit^{low} and Sca-1^{high} cells with SLAM gating to define phenotypic HSCs (pHSCs) both pre-IR and post IR (Figure 1E).

$dmPGE_2$ substantially delayed pHSC depletion at 24 h and retained higher pHSC numbers at all time points (Figure 1F). Interestingly, c-Kit loss was attenuated at 24 h and reversed by day 9 among total lineage$^-$ cells (Figure 1E, top panels) as well as on pHSCs (Figure 1G). Notably, while TNCs were only modestly higher with $dmPGE_2$ at 24 h and reached a nadir equivalent to vehicle at 72 h (Figure 1C), pHSCs were particularly preserved at these time points and increased in frequency among TNCs (Figures S3A and S3B). In contrast, CD150$^-$CD48$^+$ cells (Figure S3A), representing HPCs within the classical LSK gate (Oguro et al., 2013) but not fully defined post IR, reflected the mild TNC protection at 24 h and 72 h (Figure S3C) with no change in frequency (Figure S3D). Frequency did change at 9 days in the vehicle group due to more dramatic loss of other cell types, and was normalized in $dmPGE_2$-treated mice (Figures S3C and S3D).

Since phenotype does not always predict function (Chen et al., 2019), we evaluated long-term HSCs by competitive transplantation. Marrow from vehicle-treated mice 1 h post IR (where no reduction in pHSCs was observed) or 24 h post IR (when pHSCs were clearly reduced) were essentially unable to contribute to hematopoiesis by 16 weeks post transplant (Figure 1H). In contrast, marrow from $dmPGE_2$-treated mice contributed significantly to long-term trilineage reconstitution when harvested either 1 h or 24 h post IR. Furthermore, HPC colony-forming cells (CFCs) were significantly higher in mice that received $dmPGE_2$ compared with vehicle at all time points (Figure 1I) and after recovery of survivors (Figure 1J). These findings indicate that $dmPGE_2$ given prior to exposure significantly protects HSCs and HPCs from the effects of lethal IR.

$dmPGE_2$ Attenuates IR-Induced HSC Cycling and DNA Damage

We next investigated potential mechanisms responsible for the strong radioprotective effect of $dmPGE_2$ on HSC

Figure 1. $dmPGE_2$ Given Before Lethal IR Promotes Hematopoietic Recovery

$dmPGE_2$ or vehicle was given 30 min prior to 8.53 Gy IR.

(A) Survival post IR; n = 20 mice, $dmPGE_2$; n = 60 mice, vehicle.

(B) Time-course schema.

(C) TNC; n = 5–8 mice/group.

(D) Representative femur H&E histology; 100×; n = 3–5 mice/group in two experiments; scale bars, 50 μm.

(E) Representative wide LSK and SLAM gating for pHSCs.

(F) Number of pHSCs/mouse; n = 4–8 mice/group.

(G) Mean fluorescence intensity (MFI) of c-Kit on pHSCs; n = 5–8 mice/group.

(H) Repopulating activity at 16 weeks post transplant of marrow cells from mice 1 h (top) and 24 h (bottom) post IR, showing total chimerism (left) and trilineage contribution (right); "Trilineage Recon" is the fraction of mice/group with reconstitution of all three lineages; n = 6–8 mice/group.

(I) CFCs/mouse; n = 4–8 mice/group in two experiments.

(J) CFCs/mouse of survivors at day 35 post IR; n = 4–8 mice/group.

*$p < 0.05$, $^{\dagger}p < 0.05$ versus NI. See also Figures S1–S3. Data are mean ± SEM.

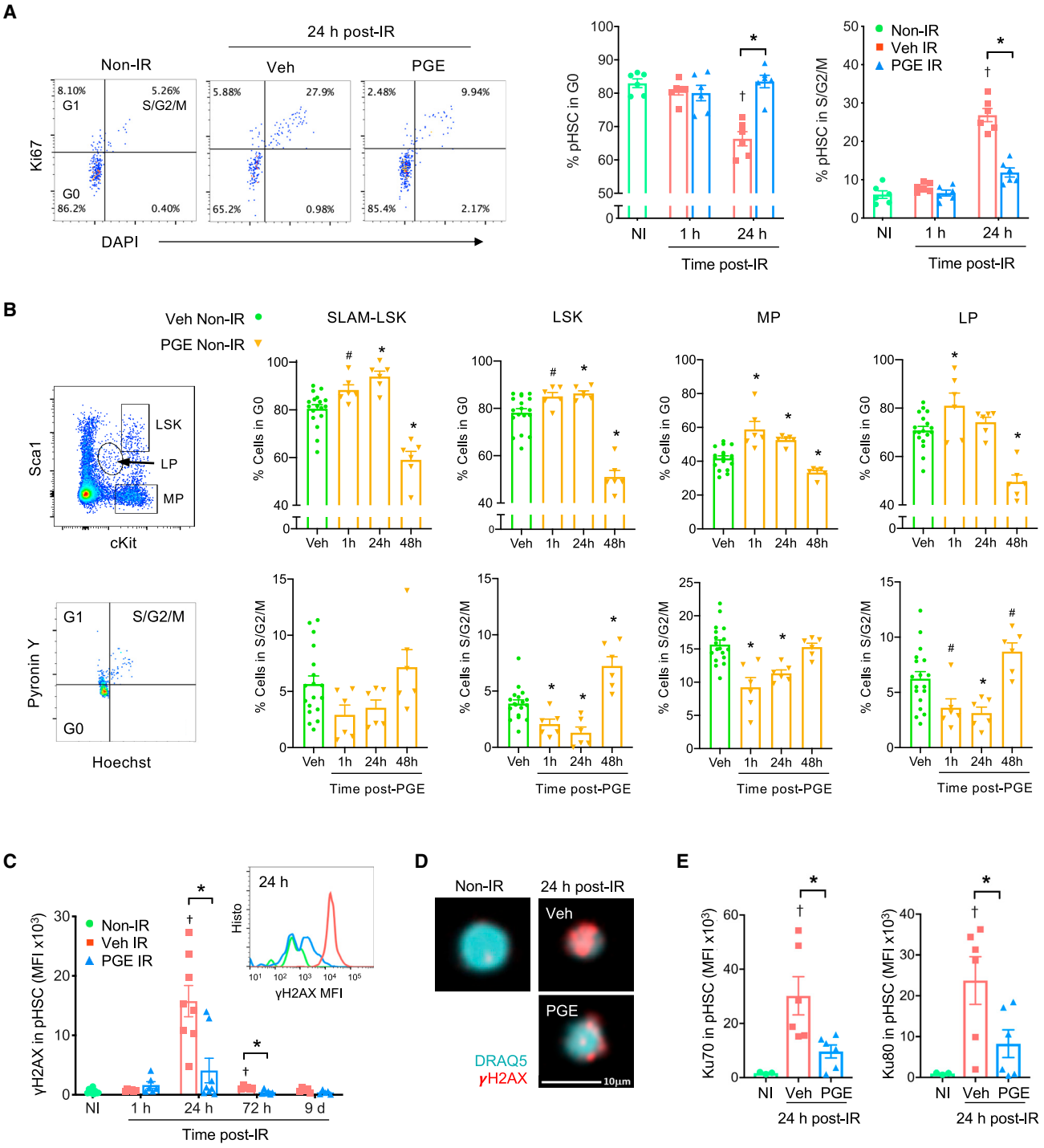

Figure 2. dmPGE$_2$ Attenuates Cycling and DNA Damage in pHSCs Post IR

(A) Representative Ki67/DAPI gating and analysis of pHSCs in G_0 or S/G_2/M at 1 h and 24 h post IR; n = 6 mice/group; *p < 0.05, †p < 0.05 versus NI.

(B) (Top left) Gating of lymphoid (LP) and myeloid (MP) progenitors along with LSK. (Bottom left) Representative pyronin Y/Hoechst gating. (Right) Cell cycle in non-IR populations post PGE. n = 6 mice/group/time point; vehicle (Veh) values from each time point were used for normalization and combined (n = 18); *p < 0.05 versus Veh; #p < 0.1 versus Veh.

(legend continued on next page)

number and function. While HPC protection is also important, loss of c-Kit restricted flow-cytometric studies post IR to the validated pHSC gate. Cell-cycle quiescence is a hallmark of HSCs, and restriction of cycling is essential to prevent HSC depletion and maintain hematopoiesis (Cheng et al., 2000). While hematopoietic stress stimulates HSC proliferation to support emergency hematopoiesis (Passegue et al., 2005), replication with unrepaired IR-induced DNA lesions can cause additional high levels of DNA double-strand breaks (DSBs) (Staszewski et al., 2008). We therefore examined HSC cell-cycle dynamics and DNA damage signaling. In vehicle-treated mice, the percentage of pHSCs in S/G_2/M phase more than tripled from non-IR levels by 24 h post IR, whereas pretreatment with $dmPGE_2$ resulted in significant preservation of the quiescent pHSC pool (Figure 2A). To test whether $dmPGE_2$ inhibits cycling independently of the irradiated environment, we investigated the effect of $dmPGE_2$ alone on cycle status over time in the non-IR setting. This also allowed analysis of populations enriched for myeloid progenitors (MPs) and lymphoid progenitors (LPs) without loss of c-Kit (Figure 2B, left). In non-irradiated mice, $dmPGE_2$ suppressed cycling of classically gated SLAM-LSK HSCs, as well as total LSK, MPs, and LPs below homeostatic levels for at least 24 h, with a subsequent surge in cycling above steady state by 48 h most likely representing a rebound effect (Figure 2B). Together, these data suggest that cell-cycle suppression by $dmPGE_2$ counteracts IR-induced HSC, and possibly HPC, proliferation during the first critical day following genotoxic insult.

To evaluate whether early suppression of HSC cell cycle correlates with less DNA damage and repair, we analyzed DNA damage response factors. Phosphorylation of ataxia telangiectasia mutated (p-ATM), one of the first events in response to DNA damage, was increased in HSCs by 1 h post IR and remained elevated through 9 days in vehicle- and $dmPGE_2$-treated mice (Figure S3E). While p-ATM qualitatively marks DNA damage, its target histone subunit H2AX is a quantitative marker for DSB sites (Mariotti et al., 2013). Phosphorylated H2AX (γH2AX) increased considerably between 1 h and 24 h post IR in HSCs from the vehicle group, while significantly less was detected in HSCs from the $dmPGE_2$ group (Figure 2C). Foci of γH2AX in each group were further visualized at 24 h by imaging cytometry, recapitulating this pattern (Figure 2D). Although γH2AX can increase during DNA replication in certain cell types, the histogram inset (Figure 2C) and pHSC images (Figure S3F) show high γH2AX in virtually all pHSCs of the 24-h vehicle group and not just the ~27% shown to be in S/G_2/M (Figure 2A). γH2AX levels decreased by 72 h, remaining higher than non-IR levels in HSCs from vehicle-treated mice, but returning to basal levels in $dmPGE_2$-treated mice. Since $dmPGE_2$ could be increasing DNA repair rather than attenuating DNA damage, we evaluated DNA-repair enzymes Ku70 and Ku80 of the non-homologous end-joining (NHEJ) pathway, the main DSB repair mechanism in HSCs (Mohrin et al., 2010). Both enzymes were significantly increased in HSCs from the vehicle group at 24 h, consistent with increased DNA damage requiring increased DNA repair, and were significantly lower in HSCs from the $dmPGE_2$ group (Figure 2E), suggesting that $dmPGE_2$ is not increasing repair but attenuating the accumulation of DNA damage. These data support a potential mechanism whereby $dmPGE_2$ attenuates further DNA damage in HSCs by preventing cell-cycle entry too early after exposure to lethal IR.

IR-Related Sequelae Are Attenuated in HSCs by $dmPGE_2$

Since $dmPGE_2$ attenuated early cell-cycle entry and accumulation of DNA damage in HSCs within 24 h post IR, sequelae of IR damage were evaluated. Cleaved poly(ADP-ribose) polymerase (PARP), a measure of apoptosis (Boulares et al., 1999), was significantly elevated by 24 h post IR in HSCs from vehicle- but not $dmPGE_2$-treated mice (Figure 3A). Cleaved PARP increased in HSCs from both groups at 72 h and 9 days, suggesting that $dmPGE_2$ mediated a delay in the onset of apoptosis in HSCs for at least 24 h. While reactive oxygen species (ROS) generated directly and immediately by IR contribute to initial DNA damage, affected mitochondria can further increase ROS levels, exacerbating cell damage (Ludin et al., 2014). $dmPGE_2$ prevented an increase in mitochondrial ROS in HSCs within the first 24 h and maintained significantly lower ROS levels throughout the time course (Figure 3B). $dmPGE_2$ also prevented an IR-induced increase in HSC mitochondrial membrane potential (Figure 3C). The transcriptional coactivator PGC-1, which regulates mitochondrial biogenesis and activity (St-Pierre et al., 2006), was significantly reduced in HSCs from 24 h through 9 days post IR, but remained significantly higher with $dmPGE_2$ (Figure 3D). IR damage also causes hematopoietic cell senescence (Botnick et al., 1979; Chua et al., 2019; Himburg et al., 2017). The fraction of HSCs expressing senescence-associated β-galactosidase (SA-β-gal) (Figure 3E) and $p16^{INK4A}$/cyclin-dependent

(C) MFI of γ-H2AX in pHSCs. Inset: representative histograms at 24 h. n = 6–8 mice/group; $^{\dagger}p < 0.05$ versus NI; $^{*}p < 0.05$.
(D) Representative pHSCs by imaging cytometry for γ-H2AX at 24 h post IR.
(E) MFI of ku70 and ku80 in pHSCs at 24 h post IR. n = 6 mice/IR group, 3/NI; $^{*}p < 0.05$.
See also Figure S3. Data are mean ± SEM.

kinase inhibitor 2A (Cdkn2a) (Figure 3F), increased in vehicle-treated mice within 24 h of IR and continued to increase through 9 days, but remained significantly lower in $dmPGE_2$-treated mice. Overall, $dmPGE_2$ delayed apoptosis, preserved mitochondrial homeostasis, attenuated ROS production, and reduced senescence in HSCs post IR.

Molecular Networks in HSCs Affected by IR and Modified by $dmPGE_2$

The radioprotective effects of $dmPGE_2$ on HSCs were manifested early, preserving long-term repopulation capacity in HSCs as early as 1 h after lethal IR. By 24 h post IR, $dmPGE_2$ had attenuated loss of pHSC numbers, early pHSC cycling and DNA damage, and other sequelae that compromise HSC function. To understand molecular networks contributing to this early protection, we performed RNA-seq on sorted pHSCs harvested 1 h and 24 h post IR from mice receiving vehicle or $dmPGE_2$ at −30 min. We utilized Fgd5 mice to enhance HSC purity post IR, gating $ZsGreen^+$ along with SLAM-LSK markers.

Multi-dimensional scaling (MDS) plots revealed strong groupwise clustering (Figure 4A). By 1 h post IR, the vehicle-treated non-IR (Veh-NI) and IR (Veh-IR) groups clustered far apart, indicating substantial IR-specific changes. In contrast, the $dmPGE_2$-treated non-IR (PGE-NI) and IR (PGE-IR) groups clustered close together, suggesting that $dmPGE_2$ dampens the impact of IR on HSC gene transcription. Among genes increased by IR >2-fold at 1 h and attenuated by $dmPGE_2$ (false discovery rate [FDR] < 0.05; total 155 genes), the most highly enriched pathways were p53 signaling and apoptosis, followed closely by tumor necrosis factor (TNF) and nuclear factor κB (NF-κB) signaling pathways (Table 1). The genes involved in the gene ontology (GO) term "apoptotic process" in Table 1 (1 h post IR) are shown in heatmap form in Figure 4B. Utilizing gene set enrichment analysis (GSEA), apoptotic signaling was again highlighted in the top scoring categories as both increased in HSCs by IR at 1 h, and attenuated with $dmPGE_2$ (Table S1; Figures 4C and 4D). NF-κB signaling scored highest by GSEA for both an increase with IR and prevention by $dmPGE_2$ (Table S1), and these scores were driven largely by expression of the NF-κB subunits themselves; multiple NF-κB subunits and inhibitors were increased by IR and attenuated with $dmPGE_2$, and some inhibitors were specifically increased by $dmPGE_2$ (Figure 4E).

We utilized Ingenuity Pathway Analysis (IPA) to identify potential upstream regulators involved in HSC IR damage and protection. IPA predicted strong IR-induced activation of TNF, with a particularly high activation *Z* score (+8.26, Figure 4F) based on the expression pattern of 194 downstream genes. Of these, 122 genes were significantly different when $dmPGE_2$ was given before IR, contributing to a predicted partial inhibition of TNF (*Z* score of −2.21, Figures 4F and S4). Quantitation of marrow TNFα indicated it was indeed increased within 1 h of IR but was not attenuated by $dmPGE_2$ (Figure 4G), suggesting that $dmPGE_2$ may alter downstream HSC responses to TNFα rather than its production. Of the TNFα receptors (TNFR1 and TNFR2), $dmPGE_2$ increased TNFR2 mRNA in HSCs within 1 h, regardless of IR exposure, while TNFR1 mRNA was unaffected (Figure S5A). Surface TNFR1 levels were lower at 1 h post IR, likely reflecting internalization, but interestingly remained high in cells from mice that received $dmPGE_2$ (Figure S5B). Consistent with the TNFR2 mRNA pattern, surface TNFR2 increased with $dmPGE_2$ relative to cells from both vehicle-treated IR and non-IR mice (Figure S5B). This suggests that $dmPGE_2$ may in part be modifying early HSC responses to an IR-induced surge in marrow TNFα.

RELA (NF-κB p65) and TP53 (p53) were the next upstream regulators predicted to be most activated by 1 h post IR and inhibited by $dmPGE_2$ (Figure 4F). NF-κB is a major mediator of TNF signaling, and both regulators involve downstream genes highly overlapping with TNF and each other, suggesting interacting signaling networks (Figure 4F, right). Of these top three regulators, p53 was most broadly inhibited by $dmPGE_2$ with a high negative *Z* score of −4.30 comparable with the IR-induced activation *Z* score of +5.44. The majority of genes contributing to these scores are known to be upregulated by p53, and were increased by IR but remained significantly lower with $dmPGE_2$ pretreatment (Figure 4H). Some genes known to be downregulated by p53 also contributed to these scores, becoming decreased with IR but not with $dmPGE_2$ pretreatment (Figure 4H, bottom cluster). The IR-upregulated genes downstream of p53 predominantly encode known apoptosis-promoting molecules such as *Aen* (apoptosis-enhancing nuclease), *Bbc3* (BCL2 binding component 3), *Cdkn1a* (cyclin-dependent kinase inhibitor 1A, $p21^{CIP1/WAF1}$, (p21)), *Eda2r* (ectodysplasin A2 receptor), *Ei24* (etoposide induced 2.4 mRNA), *Fas* (TNF receptor superfamily member 6), *Phlda3* (plecktrin homology like domain, family A, member 3), *Sesn2* (sestrin 2), and *Trp53inp1* (tumor protein p53-inducible nuclear protein 1). These also included negative feedback molecules such as *Birc3* (baculoviral IAP repeat-containing 3), *Ccng1* (cyclin G1), *Ddias* (DNA damage induced apoptosis suppressor), *Mdm2* (transformed mouse 3T3 cell double minute 2), and *Ppm1d* (protein phosphatase 1D magnesium-dependent, delta isoform).

Relative expression levels of p53-signature genes were confirmed by single-cell qRT-PCR in pHSCs purified from wild-type mice 1 h post IR. Principal component analysis (PCA) of single cells recapitulated the three-way groupwise clustering (Figure 4I), and corresponding gene expression effects were observed at the level of individual HSCs

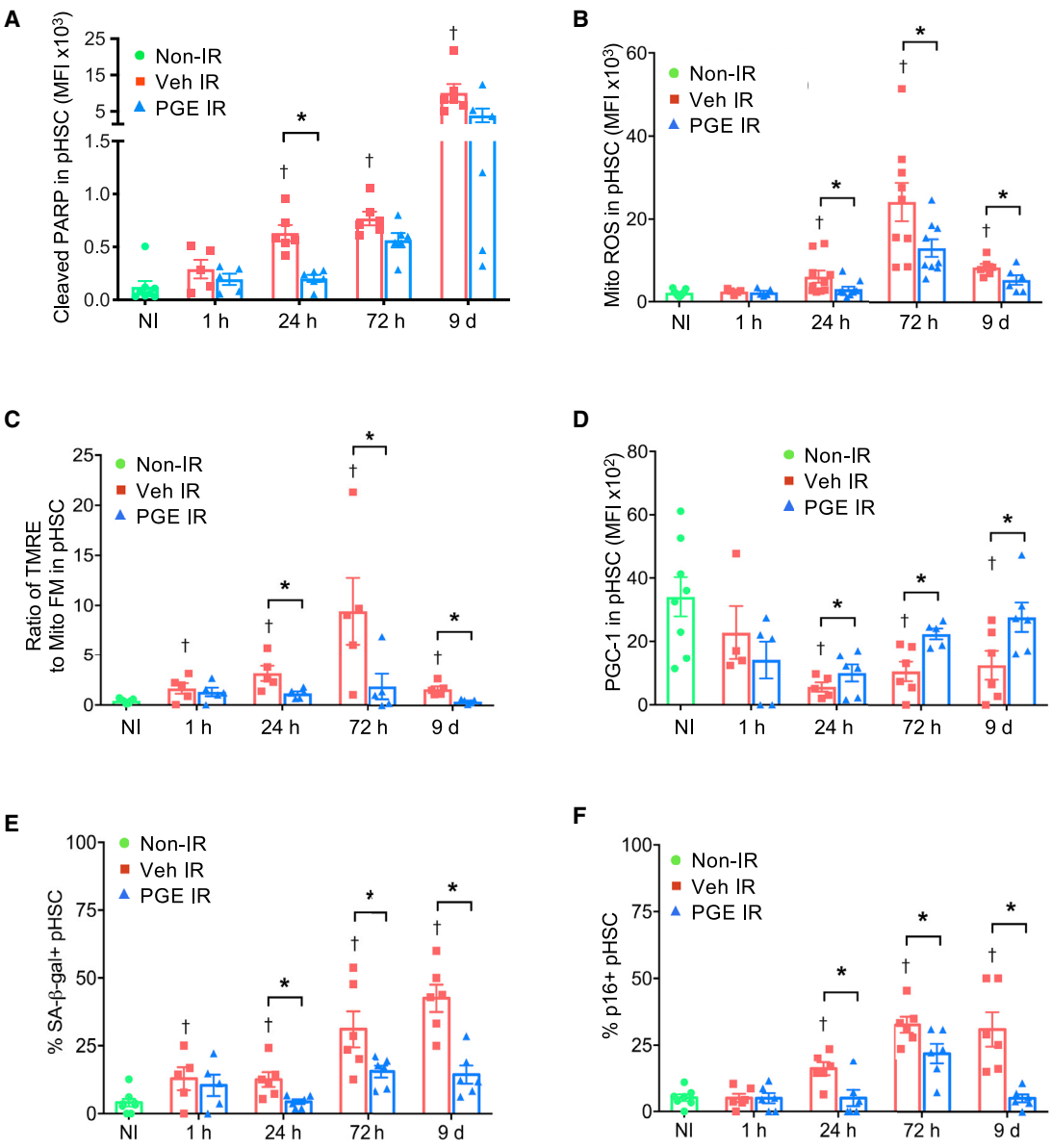

Figure 3. Sequelae of IR Are Attenuated in pHSCs by dmPGE$_2$

Apoptosis, mitochondrial activity, and senescence analyzed in pHSC-gated cells post IR.

(A) MFI of cleaved PARP; n = 5–6 mice/group.

(B) MFI of mitochondrial ROS; n = 5–9 mice/group.

(C) Mitochondrial membrane potential expressed as MFI ratio of TMRE to Mito Tracker Green; n = 4–5 mice/group.

(D) MFI of PGC-1; n = 4–8 mice/group.

(E and F) Percent positive for (E) SA-β-gal and (F) p16; n = 5–6 mice/group.

*p < 0.05, †p < 0.05 versus NI. Data are mean ± SEM.

(Figure 4J). Upregulation of Fas, an apoptotic surface protein induced by p53 in response to DNA damage (Muller et al., 1998), was confirmed at the protein level by flow cytometry, roughly doubling on HSCs by 3 h post IR and reaching >5-fold by 24 h (Figure 4K). In agreement with the mRNA findings by RNA-seq (Figure 4H, ninth from bottom), the increase in Fas surface protein was attenuated by dmPGE$_2$ (Figure 4L). Thus, dmPGE$_2$ radioprotection interferes with signaling networks downstream of TNF, NF-κB, and p53 initiated almost immediately in HSCs by lethal IR, predominantly blocking p53 activation and apoptotic signaling by 1 h post IR.

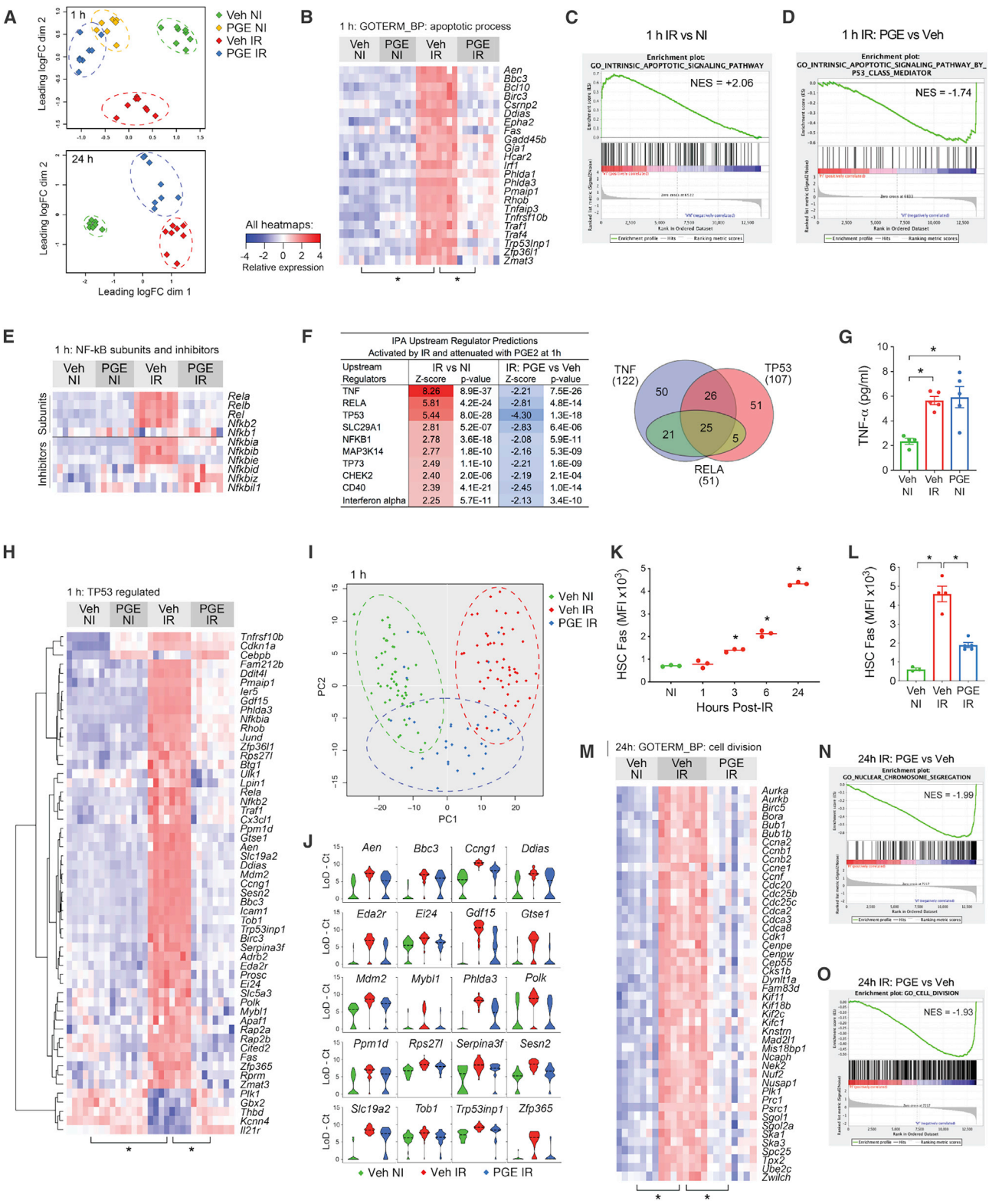

Figure 4. dmPGE$_2$ Blocks IR-Induced Gene Expression at 1 h and 24 h Post IR in HSCs

HSCs were sorted from dmPGE$_2$- or vehicle-treated Fgd5 mice (ZsGr + pHSC) 1 h or 24 h post IR.

(A) RNA-seq MDS plots at 1 h and 24 h; n = 7–8 mice/group.

(legend continued on next page)

Transcriptional Effects of dmPGE$_2$ Alone in HSCs Prior to IR

Pathways induced by dmPGE$_2$ prior to IR may be "priming" HSCs to respond differently upon exposure to IR, and could represent protective factors. In addition, we explored whether dmPGE$_2$ affects HSCs by direct signaling, and through which PGE$_2$ receptor(s). dmPGE$_2$ given up to 3 h prior to lethal IR is still fully radioprotective (unpublished data); thus, the non-IR dmPGE$_2$ group at the 1 h time point—corresponding to 1.5 h post dmPGE$_2$ injection—was analyzed for protective transcriptional activity. Of note, the single most significant gene effect in HSCs by dmPGE$_2$ alone was a 17-fold increase in the cell-cycle inhibitor p21 (FDR = 5.6×10^{-81}), corresponding to the observed cell-cycle suppression with dmPGE$_2$ alone (Figure 2B). In total, 888 genes with >1.4-fold change and FDR < 0.05 were utilized by IPA to predict the transcriptional regulators most likely activated in HSCs by dmPGE$_2$ alone (Table 2). Atop the list was cyclic AMP (cAMP)-responsive element binding protein 1 (CREB1), a known transcriptional mediator of PGE$_2$ signaling through EP2 and EP4 (Fujino et al., 2005), supporting HSC-intrinsic dmPGE$_2$ signaling through one or both receptors. While EP2 mRNA was virtually undetectable in HSCs by RNA-seq, EP4 was highly expressed (Figure S6A). Also, of all PGE$_2$ receptors, only EP4 mRNA levels were affected by dmPGE$_2$ (decreased) or IR (increased) (Figure S6B). Furthermore, based on known EP4 downstream gene expression patterns, IPA predicted that EP4 activity was decreased by IR (Z score −2.34, p = 3.2×10^{-9}) but preserved by dmPGE$_2$ (Z score 2.48, p = 1.2×10^{-10}); EP4 downstream genes common to both Z scores and also affected by dmPGE$_2$ alone are shown in Figure S6C. This analysis suggests that dmPGE$_2$ acts directly on HSCs, likely through EP4, and provides candidate protective transcriptional regulators (Table 2) for further study.

Cell-Cycle Genes Dominate 24-h Transcriptional Effects in HSCs

Initial IR-induced TNF/NF-κB and p53 gene signatures were short lived in HSCs, with most returning to basal levels at 24 h post IR (Figure S4). At 24 h, the predominant transcriptional effect of IR on surviving HSCs was an increase in cell-cycle genes, which was significantly prevented by dmPGE$_2$. Genes increased by IR >2-fold at 24 h and attenuated with dmPGE$_2$ (both at FDR < 0.05; total 164 genes) were enriched for terms such as mitosis, cell division, mitotic nuclear division, centromere, and others almost exclusively related to cell cycle (Table 1, 24 h post IR). The individual genes associated with the GO term "cell division" are shown in Figure 4M. GSEA also identified primarily cell-cycle-related categories as attenuated in HSCs with dmPGE$_2$ (Table S2; Figures 4N and 4O). IPA predicted that dmPGE$_2$ also increased cellular functions related to homeostasis and hematopoietic capacity relative to vehicle at 24 h, while attenuating DNA replication/repair-related activity (Table 3). Overall, dmPGE$_2$ preserved HSC homeostasis genes and prevented the increase in cell-cycle genes by 24 h post IR, supporting the dmPGE$_2$-mediated inhibition of HSC cycling observed by flow cytometry at 24 h post IR and in the non-IR setting (Figures 2A and 2B).

DISCUSSION

Understanding tissue-specific radioprotective mechanisms is important for the development of therapies for intentional or accidental radiation exposures and for protection during future endeavors beyond the earth's protective magnetic field. In this study, we performed phenotypic, functional, and genomic analyses of primitive hematopoietic cells with and without dmPGE$_2$ radioprotection in a

(B) Heatmap of genes associated with GO term "apoptotic process" (DAVID Functional Annotation analysis) from the 1-h RNA-seq (Table 1). *All genes FDR < 0.05 between indicated groups.
(C) GSEA plot for GO term "intrinsic apoptotic signaling pathway" in Veh-IR versus Veh-NI at 1 h (Table S1). NES, normalized enrichment score.
(D) GSEA plot for GO term "intrinsic apoptotic signaling pathway by p53 class mediator" in PGE-IR versus Veh-IR at 1 h (Table S1).
(E) Heatmap of NF-κB subunits and inhibitors at 1 h.
(F) Upstream regulators predicted by IPA as activated by IR and attenuated with dmPGE$_2$ in HSCs at 1 h post IR. Color intensity, prediction strength for activation (red) or inhibition (blue); p value, significance of gene set overlap.
(G) TNFα in marrow supernatants 1 h post IR; n = 4–5 mice/group; *p < 0.01.
(H) Heatmap of the most significant (*FDR < 0.001) TP53-regulated genes at 1 h contributing to predictions in (F).
(I and J) Single-cell qRT-PCR for genes from the TP53 signature in pHSCs 1 h post IR; n = 3 mice combined/group. (I) PCA plot of a single HSC. (J) Relative gene expression in a single HSC. All p < 0.05 for both Veh-IR versus Veh-NI and Veh-IR versus PGE-IR by Kruskal-Wallis test with Dunn's correction. LoD, limit of detection; Ct, threshold cycle.
(K) MFI of Fas on pHSCs; n = 3 mice/group; *p < 0.05 versus NI.
(L) MFI of Fas on pHSCs 24 h post IR; n = 3–5 mice/group; representative of three experiments.
(M) 24-h RNA-seq genes (*FDR < 0.05) associated with GO term "cell division" (DAVID Functional Annotation analysis) (Table 1).
(N and O) 24-h RNA-seq GSEA plots for (N) GO term "nuclear chromosome segregation" and (O) GO term "cell division" (Table S2).
See also Figures S4–S6. Data are mean ± SEM.

Table 1. Top 10 Functional Annotation Enrichments among Genes Increased by Irradiation >2-Fold and Attenuated with $dmPGE_2$

Term	Category	Term ID	Count	Fold Enrichment	Benjamini p Value
1 h Post IR					
p53 signaling pathway	KEGG_PATHWAY	mmu04115	12	19	1.7×10^{-9}
Apoptosis	UP_KEYWORDS	NA	20	6	7.3×10^{-8}
apoptotic process	GOTERM_BP_DIRECT	GO:0006915	23	6	1.3×10^{-7}
TNF signaling pathway	KEGG_PATHWAY	mmu04668	12	12	1.9×10^{-7}
NF-κB signaling pathway	KEGG_PATHWAY	mmu04064	11	12	5.6×10^{-7}
inflammatory response	GOTERM_BP_DIRECT	GO:0006954	16	6	1.5×10^{-5}
Epstein-Barr virus infection	KEGG_PATHWAY	mmu05169	12	6	1.0×10^{-4}
NIK/NF-κB signaling	GOTERM_BP_DIRECT	GO:0038061	4	110	6.7×10^{-4}
I-κB kinase/NF-κB signaling	GOTERM_BP_DIRECT	GO:0007249	6	26	6.9×10^{-4}
response to cytokine	GOTERM_BP_DIRECT	GO:0034097	8	14	7.1×10^{-4}
24 h Post IR					
Mitosis	UP_KEYWORDS	NA	43	23	3.0×10^{-43}
Cell division	UP_KEYWORDS	NA	47	18	2.3×10^{-42}
Cell cycle	UP_KEYWORDS	NA	54	12	8.0×10^{-41}
Mitotic nuclear division	GOTERM_BP_DIRECT	GO:0007067	44	20	8.2×10^{-41}
Cell division	GOTERM_BP_DIRECT	GO:0051301	46	15	4.4×10^{-38}
Cell cycle	GOTERM_BP_DIRECT	GO:0007049	51	10	1.5×10^{-34}
Centromere	UP_KEYWORDS	NA	25	26	1.6×10^{-25}
Kinetochore	GOTERM_CC_DIRECT	GO:0000776	25	26	5.1×10^{-25}
Chromosome, centromeric region	GOTERM_CC_DIRECT	GO:0000775	25	22	1.6×10^{-23}
Cytoskeleton	UP_KEYWORDS	NA	48	6	2.7×10^{-23}

Top 10 enrichments assessed by DAVID bioinformatics tool.
All genes FDR < 0.05 for both increase with Veh-IR versus Veh-NI and decrease with PGE-IR versus Veh-IR; 155 genes at 1 h, 164 genes at 24 h.

controlled murine model of H-ARS (Plett et al., 2012). Our findings provide a prospective analysis of stem cells with differing capacities to survive radiation exposure and represent the first study with this approach in HSCs. We confirm that treatment with $dmPGE_2$ before lethal IR increases survival (Steel et al., 1988; Walden et al., 1987) and protects hematopoiesis as previously described in the sublethal setting (Hanson and Ainsworth, 1985; Walden et al., 1987). We present a detailed evaluation of the effects of $dmPGE_2$ on primitive hematopoietic cells and its potential mechanisms of action.

Lethal IR results in a significant increase in HSC proliferation by 24 h, accompanied by an increase in DNA DSB between 1 h and 24 h post IR. $dmPGE_2$ given prior to IR attenuated both IR-induced cycling and DNA damage in HSCs, delayed apoptosis, and attenuated the progression of mitochondrial compromise, mitochondrial ROS production, and senescence in surviving cells. By transcriptomic analysis, $dmPGE_2$ predominantly attenuated induction of p53-associated apoptotic genes within 1 h of IR, and attenuated the increase in cell-cycle genes at 24 h. An integrated model of $dmPGE_2$ radioprotection in HSCs is proposed in Figure S7.

HSC cell cycle/quiescence is held in delicate balance, with low proliferation rates essential for maintenance and self-renewal (Hao et al., 2016; Seita and Weissman, 2010). However, HSCs are "poised" to rapidly enter the cell cycle in response to stress (Cheung and Rando, 2013; Passegue et al., 2005). Accordingly, rapid induction of HSC cycling was observed within 24 h post IR. However, attempted DNA replication immediately after IR exposure, before repair of DNA lesions (Georgakilas et al., 2004; Sage and

Table 2. Top 10 Transcription Regulators with Predicted Activation in HSCs by dmPGE$_2$ Alone

Symbol	Name	*Z* Score	p Value	No. of Genes
CREB1	cAMP responsive element binding protein 1	5.23	6.9×10^{-13}	59
STAT3	signal transducer and activator of transcription 3	3.44	2.9×10^{-13}	58
SMAD3	SMAD family member 3	3.38	1.9×10^{-5}	23
CREM	cAMP responsive element modulator	3.36	1.1×10^{-16}	33
NUPR1	nuclear protein 1	3.24	1.8×10^{-8}	46
STAT6	signal transducer and activator of transcription 6	3.09	4.3×10^{-8}	32
FOXL2	forkhead box L2	3.00	3.9×10^{-6}	12
TP63	tumor protein p63	2.95	5.7×10^{-6}	33
EGR1	early growth response 1	2.82	5.5×10^{-13}	31
TCF7L2	transcription factor 7 like 2	2.78	1.2×10^{-3}	24

Predicted activation by Ingenuity Pathway upstream regulators analysis. Measured at 1.5 h post injection, no IR.

Shikazono, 2017), can result in further DSB formation and cell death (Staszewski et al., 2008). DNA damage increased in HSCs over the first 24 h post IR, but both HSC cycling and DNA DSB formation were attenuated by dmPGE$_2$. Maintenance of HSC quiescence by dmPGE$_2$ may be significant for protection, since the portion of HSCs in active cell cycle is less capable of reconstitution upon transplant into the lethally irradiated environment compared with those in G_0/G_1 (Fleming et al., 1993). The observation that dmPGE$_2$ alone increases p21 and suppresses HSC/HPC cycling within 1 h also raises the possibility that increased quiescence prior to IR allows for less immediate DNA damage. However, while NHEJ occurs in all cell-cycle phases, a higher-fidelity DNA-repair mechanism (homologous recombination) increases in cycling HSCs/HPCs exposed to low-dose IR (Mohrin et al., 2010), suggesting that HSCs irradiated while in cycle may have better quality of repair. The extreme conditions of high-dose IR may alter this paradigm, but this merits further study in the context of dmPGE$_2$ radioprotection. Overall, cell-cycle suppression by dmPGE$_2$ likely plays a significant radioprotective role.

We reported that PGE$_2$ inhibits proliferation of HPCs after *in vivo* administration (Gentile et al., 1983; Gentile and Pelus, 1987). We now identify a temporary reduction in HSC and HPC cycling for ~24 h following a single dmPGE$_2$ dose, with a subsequent rebound in cycling above steady-state levels by 48 h. Thus, differing PGE$_2$ dosing regimens and analysis time points may indicate either suppression or activation of cycling. In addition, we and others have shown that dmPGE$_2$ increases HSC cycling following short-pulse exposure *in vitro* (Hoggatt et al., 2009; North et al., 2007; Pelus, 1982; Pelus and Hoggatt, 2011), illustrating that microenvironment is another important factor for HSCs, and also for a pleiotropic bioactive lipid such as dmPGE$_2$. Regarding IR, we showed that dmPGE$_2$ given shortly after IR is radiomitigating, while an increase in marrow PGE$_2$ at later time points inhibits hematopoietic regeneration (Hoggatt et al., 2013b). Together, these data suggest that HSC and HPC cycling on the first day of IR exposure is likely deleterious and is attenuated by dmPGE$_2$, while subsequent cycling is essential for regeneration, and dmPGE$_2$ given pre-IR may play a time-sensitive role.

P53 apoptotic signaling is well established in the cellular IR response (Alvarez et al., 2006; Fei et al., 2002; Lee et al., 2015). Apoptosis plays a central role in H-ARS post IR, and p53 signaling is a known HSC response to genotoxic stress (Shao et al., 2014; Yu et al., 2010). Interestingly, high p53 levels are maintained in HSCs at steady state and support quiescence (Liu et al., 2009). This likely accounts for the rapid induction of p53 activity in HSCs post IR, while its quiescence function is likely overridden by hematopoietic stress. Recent transcriptome analysis of primarily B-lineage cells identified p53 signaling as the most enriched pathway induced by IR, albeit at sublethal IR of 1–2 Gy, with apoptosis as the most enriched GO category (Pawlik et al., 2011). This p53 transcriptional response was confirmed and extended in our study to lethal IR, and expanded in depth for HSCs. RNA-seq analysis identified 161 total p53-regulated genes as significantly affected by IR, the majority of which (107) were attenuated by dmPGE$_2$. *Bbc3*, also known as Puma (p53 upregulated mediator of apoptosis), was one such gene upregulated in HSC at 1 h and blocked by dmPGE$_2$. Puma deletion in mice confers striking survival from lethal IR, more so than total p53 deletion, protecting HSCs from cell death and functional compromise (Yu et al., 2010). Thus, Puma

Table 3. Cellular Functions 24 h Post IR Predicted Increased or Decreased in HSCs with $dmPGE_2$

Functions Annotation	Category	*Z* Score	Predicted Activation State	p Value	No. of Genes
Cellular homeostasis	cellular function and maintenance	4.98	increased	2×10^{-11}	218
Hematopoiesis of mononuclear leukocytes	hematopoiesis	4.54	increased	2×10^{-14}	122
Lymphopoiesis	hematopoiesis	4.34	increased	9×10^{-14}	115
Homeostasis of leukocytes	cellular function and maintenance	4.31	increased	2×10^{-13}	103
Cell movement	cellular movement	4.28	increased	6×10^{-23}	327
Lymphocyte homeostasis	cellular function and maintenance	4.07	increased	6×10^{-12}	98
Migration of cells	cellular movement	4.02	increased	1×10^{-22}	298
T cell homeostasis	hematological system development and function	3.89	increased	7×10^{-12}	94
Microtubule dynamics	cellular function and maintenance	3.76	increased	1×10^{-11}	174
Organization of cytoplasm	cellular function and maintenance	3.76	increased	7×10^{-14}	221
Alignment of chromosomes	DNA replication, recombination, and repair	−2.67	decreased	8×10^{-15}	18
Metabolism of DNA	DNA replication, recombination, and repair	−2.16	decreased	5×10^{-10}	68
Repair of DNA	DNA replication, recombination, and repair	−2.12	decreased	2×10^{-11}	60

Predicted increase or decrease by Ingenuity Pathway diseases and functions analysis.
Showing top 10 predictions for "Increased" and all three predictions for "Decreased" in PGE-IR versus Veh-IR.

suppression may be a major component of the $dmPGE_2$ radioprotective mechanism.

It has been suggested that HSCs are uniquely more resistant to IR-induced p53 activation through rapid induction of p21 functioning to quench p53 phosphorylation by 6 h post IR, at least in a sublethal setting (Insinga et al., 2013). We also found that the lethal IR-induced p53 gene signature was early and transient in HSCs, strongly observable at 1 h but dissipated by 24 h post IR, and IR alone induced an 86-fold increase in p21 expression in HSCs by 1 h (FDR = 6.6×10^{-168}). However, $dmPGE_2$ alone induced a 17-fold increase in p21 in HSCs (FDR = 5.6×10^{-81}), meaning it would already be elevated in HSCs at the time of IR. Thus, rather than IR-induced p21 quickly reversing the activation of p53 as described (Insinga et al., 2013), $dmPGE_2$-induced p21 expression pre-IR could be preventing the initial p53 activation.

Activation of CREB1 represents another potential molecular mechanism of p53 attenuation in HSCs. PGE_2 signaling stimulates cAMP, which binds to cAMP-dependent protein kinase A (PKA), releasing its catalytic subunits to activate nuclear CREB (Mayr and Montminy, 2001). CREB1 had the highest *Z* score of activation in HSCs with $dmPGE_2$ alone. Activated CREB interacts with CREB binding protein (CBP) and its paralog p300 (CBP/p300) to facilitate transcription of its target genes. Intriguingly, both CREB and p53, as well as NF-κB, are among multiple transcription factors that must compete for binding to limiting amounts of cellular CBP/p300 (Dyson and Wright, 2016; Parry and Mackman, 1997). Thus, a limited supply of CBP/p300 may be sequestered by CREB at the time of IR, rendering it unavailable to p53 as well as NF-κB. Further investigation of this mechanism could lead to novel radioprotectants, since >400 proteins interact with CBP/p300 and provide competition for these limiting cofactors (Bedford et al., 2010).

TNFα production by bone marrow cells increases after IR and induces hematopoietic cell apoptosis, while TNF neutralization or knockout is protective (Cachaco et al., 2010). Our findings support this mechanism in HSCs, identifying a strong gene signature of TNF activation and >2-fold increase in marrow TNFα concentration at 1 h post IR. While $dmPGE_2$ given prior to IR partially attenuated the TNF gene signature, it did not inhibit the increase in marrow TNFα. TNFR2 mRNA and surface expression was significantly increased by $dmPGE_2$ at the 1-h time point. Unlike TNFR1, TNFR2 does not possess a "death domain" and is more associated with pro-survival signaling (Faustman and Davis, 2013; Naude et al., 2011). Furthermore, TNFR2 is associated with protection from oxidative stress (Fischer et al., 2011; Maier et al., 2013). These TNF mechanisms remain to be explored, but it is likely that

dmPGE$_2$-induced upregulation of TNFR2 contributes to an overall healthier HSC response to IR-induced TNFα. Interestingly, in the non-IR context, HSCs possess a unique TNFα response that inhibits necroptosis while pushing HSCs into cell cycle and myeloid regeneration (Yamashita and Passegue, 2019). These anti-necroptosis signals abrogate toxicity of TNFα itself but are likely inept against the toxicity of lethal IR. However, the latter function raises the possibility that TNFα mediates the IR-induced HSC cycling activation. By this model, alteration of TNF signaling by dmPGE$_2$ as observed here may link to its cycling suppression of IR-damaged HSCs.

In summary, this study elucidates cellular and molecular events occurring in HSCs during dmPGE$_2$ radioprotection from H-ARS. In particular, dmPGE$_2$ appears to block initiation of the p53-regulated apoptotic program in HSCs within 1 h post IR and attenuates HSC entry into the cell cycle within the first critical day post IR (Figure S7). These functions appear to prevent excess HSC compromise and preserve repopulating capacity early after IR, ultimately allowing for hematopoietic recovery and survival from an otherwise lethal IR exposure.

EXPERIMENTAL PROCEDURES

Mice

Indiana University School of Medicine IACUC approved all studies. SPF C57BL/6 (CD45.2) mice (Jackson Labs, Bar Harbor, ME) were received at 10 weeks old, acclimated for 2 weeks, and used at 12 weeks old. BoyJ (CD45.1) (B6.SJL-Ptprc) mice were bred in the IUSCC *In Vivo* Therapeutics Core facility. Fgd5-ZsGreen mice (C57BL/6N-Fgd5^{tm2Djr}/J) were from Jackson and bred in-house. Further information is provided in Supplemental Experimental Procedures.

Irradiation

Mice were placed in single chambers of a Plexiglas IR device and exposed to a uniform total body γ-IR dose of 8.53 Gy for IR studies, and 11-Gy split dose for transplant recipients 1 day prior to transplant. Further information is available in Supplemental Experimental Procedures.

dmPGE$_2$

dmPGE$_2$ in methyl acetate was from Cayman Chemicals (Ann Arbor, MI) and was stored at −20°C. Prior to use, dmPGE$_2$ was evaporated to dryness on ice under N_2 and reconstituted in 100% EtOH at 0.1 mg/mL. Mice received a single subcutaneous injection of 35 μg of dmPGE$_2$ or EtOH (3.5%) in 100 μL of saline 30 min before irradiation.

Histology

Femurs were fixed overnight in 4% paraformaldehyde, decalcified in 10% EDTA for 7 days, and paraffin-embedded. Five-micrometer slices were stained with hematoxylin and eosin (H&E) as described in Hoggatt et al. (2013a).

Flow Cytometry

Samples were analyzed with an LSRII flow cytometer (BD Biosciences, San Jose, CA). Cell sorting was performed on a BD SORP Aria.

Cell Isolation and Staining

Bone marrow cells were stained with an amine-reactive live/dead dye (Invitrogen LIVE/DEAD Fixable Dead Cell Stain kit; Thermo Fisher, Waltham, MA) followed by antibodies to HSC markers for gating Lineage$^-$, Sca-1$^+$, c-Kit$^+$, CD150$^+$, and CD48$^-$. The pan-WBC markers CD45, CD34, and Flt3 were included in some cases. Further antibody and staining information is provided in Supplemental Experimental Procedures. Total HSCs/mouse was calculated by multiplying pHSC frequency by TNC, and was adjusted according to the fraction of total marrow mass represented by the utilized bones (Boggs, 1984).

Colony-Forming Cell Assay

CFCs were quantitated as described by Hoggatt et al. (2013a). TNCs from non-IR mice were plated at 2 × 10^4 per 35-mm dish in triplicate in ColonyGEL Mouse Complete Medium (Reach Bio, Seattle, WA). Cells from IR mice were plated at 0.5–1 × 10^6 per dish. CFU-GEMM, CFU-GM, and BFU-E were scored microscopically after 7 days at 37°C, 5% CO_2, and 5% O_2.

Bone Marrow Transplantation

Bone marrow cells from C57BL/6 mice (CD45.2) were admixed with bone marrow cells from Boy/J mice (CD45.1) for competitive transplant into lethally irradiated Boy/J mice. Further information is provided in Supplemental Experimental Procedures.

Cell Cycle

Ten million bone marrow cells/mouse were stained for HSC markers, fixed and permeabilized, and stained with either anti-Ki-67 antibody and 1 μg/mL DAPI, or with pyronin Y and Hoechst 33342, as described by Chitteti and Srour (2014).

Mitochondrial Function

Bone marrow cells were stained for HSC markers. For mitochondrial ROS detection, cells were incubated with 100 nM Mito DCFDA ROS (Molecular Probes) for 30 min at 37°C. Mitochondrial membrane potential was analyzed following incubation with 100 nM tetramethylrhodamine ethyl ester in PBS (TMRE; Molecular Probes) for 20 min at 37°C. To estimate mitochondrial mass, 100 nM Mito Tracker Green FM (Molecular Probes) was added together with TMRE. The ratio of TMRE/Mito FM was used as the final measure of mitochondrial membrane potential.

SA-β-Gal Staining

Senescence-associated β-galactosidase (SA-β-gal) was analyzed using the FluoReporter *lacZ* Flow Cytometry Kit (Molecular Probes) as directed. Bone marrow cells were stained for HSC markers and suspended with *lacZ* staining medium at10^7 cells/mL. One hundred microliters of pre-warmed 2 mM fluorescein β-D-galactopyranoside was added to 100 μL of cells and placed in a 37°C water bath for 1 min. The reaction was stopped by adding ice-cold staining medium and analyzed by flow cytometry.

ELISA

TNFα in bone marrow supernatants was quantitated by Mouse TNFα High Sensitivity ELISA (Thermo Fisher). Further information is available in Supplemental Experimental Procedures.

HSC Sorting and RNA Sequencing

Bone marrow from Fgd5 mice was lineage depleted (EasySep Mouse Hematopoietic Progenitor Cell Isolation kit; STEMCELL Technologies) and stained for HSC markers. Viable HSCs were gated by SLAM-LSK and ZsGreen^{+} (Fgd5) and sorted into lysis buffer for RNA extraction using the RNeasy Plus Micro Kit (Qiagen, Hilden, Germany). Sequencing was performed using the HiSeq4000 system (Illumina). Further information is provided in Supplemental Experimental Procedures.

Quantitative PCR

Single-cell qRT-PCR was performed using the Fluidigm C1 and Biomark systems (San Francisco, CA). Primer probes are shown in Table S3. Further information is provided in Supplemental Experimental Procedures.

Statistics

All data are shown as mean ± SEM. Student's t tests were performed for statistical analysis between two groups. One-way ANOVA with Dunnett's test was used to compare three or more groups, and to compare two or more groups with a single control group. Statistical analysis was performed using Microsoft Excel and GraphPad Prism 8.

Data and Code Availability

The accession number for the RNA sequencing data generated in this paper is GEO: GSE151799.

SUPPLEMENTAL INFORMATION

Supplemental Information can be found online at https://doi.org/10.1016/j.stemcr.2020.07.004.

AUTHOR CONTRIBUTIONS

All authors assisted in this study. A.M.P. and L.L. designed and performed experiments, analyzed and interpreted data, prepared figures, and wrote the manuscript. K.S.M. performed and interpreted histologic analyses. C.H.S., P.A.P., H.L., M.L.C., and P.S. performed experiments. J.H. consulted on study design and edited the manuscript. C.M.O. conceptualized studies, designed experiments, evaluated data, and edited the manuscript. L.M.P. conceptualized studies, designed and performed experiments, evaluated all data, and wrote the manuscript.

ACKNOWLEDGMENTS

This work was supported by DOD partnering grant W1XWH-15-1-0254 (L.M.P.) and W1XWH-15-1-0255 (C.M.O.), and NIH grant HL096305 (L.M.P.). A.M.P. was supported by NIH T32 training grant HL007910. Flow cytometry and single-cell qRT-PCR were performed at the Flow Cytometry Resource Facility of the IU Simon Cancer Center (NCI grant P30 CA082709). The Center of Excellence Grant in Molecular Hematology (PO1 DK090948) also supported flow cytometry. The Center for Medical Genomics at IU School of Medicine, a core facility of the Indiana CTSI, performed sequencing. We thank Drs. Hal Broxmeyer and Yan Liu, IU School of Medicine, for critically reviewing the manuscript.

Received: January 18, 2020
Revised: July 2, 2020
Accepted: July 3, 2020
Published: July 30, 2020

REFERENCES

Alvarez, S., Drane, P., Meiller, A., Bras, M., Deguin-Chambon, V., Bouvard, V., and May, E. (2006). A comprehensive study of p53 transcriptional activity in thymus and spleen of gamma irradiated mouse: high sensitivity of genes involved in the two main apoptotic pathways. Int. J. Radiat. Biol. *82*, 761–770.

Bedford, D.C., Kasper, L.H., Fukuyama, T., and Brindle, P.K. (2010). Target gene context influences the transcriptional requirement for the KAT3 family of CBP and p300 histone acetyltransferases. Epigenetics *5*, 9–15.

Boggs, D.R. (1984). The total marrow mass of the mouse: a simplified method of measurement. Am. J. Hematol. *16*, 277–286.

Botnick, L.E., Hannon, E.C., and Hellman, S. (1979). A long lasting proliferative defect in the hematopoietic stem cell compartment following cytotoxic agents. Int. J. Radiat. Oncol. Biol. Phys. *5*, 1621–1625.

Boulares, A.H., Yakovlev, A.G., Ivanova, V., Stoica, B.A., Wang, G., Iyer, S., and Smulson, M. (1999). Role of poly(ADP-ribose) polymerase (PARP) cleavage in apoptosis. Caspase 3-resistant PARP mutant increases rates of apoptosis in transfected cells. J. Biol. Chem. *274*, 22932–22940.

Cachaco, A.S., Carvalho, T., Santos, A.C., Igreja, C., Fragoso, R., Osorio, C., Ferreira, M., Serpa, J., Correia, S., Pinto, d.O.P., and Dias, S. (2010). TNF-alpha regulates the effects of irradiation in the mouse bone marrow microenvironment. PLoS One *5*, e8980.

Chen, Y., Yao, C., Teng, Y., Jiang, R., Huang, X., Liu, S., Wan, J., Broxmeyer, H.E., and Guo, B. (2019). Phorbol ester induced ex vivo expansion of rigorously-defined phenotypic but not functional human cord blood hematopoietic stem cells: a cautionary tale demonstrating that phenotype does not always recapitulate stem cell function. Leukemia *33*, 2962–2966.

Cheng, T., Rodrigues, N., Shen, H., Yang, Y., Dombkowski, D., Sykes, M., and Scadden, D.T. (2000). Hematopoietic stem cell quiescence maintained by p21cip1/waf1. Science *287*, 1804–1808.

Cheung, T.H., and Rando, T.A. (2013). Molecular regulation of stem cell quiescence. Nat. Rev. Mol. Cell Biol. *14*, 329–340.

Chitteti, B.R., and Srour, E.F. (2014). Cell cycle measurement of mouse hematopoietic stem/progenitor cells. Methods Mol. Biol. *1185*, 65–78.

Chua, H.L., Plett, P.A., Fisher, A., Sampson, C.H., Vemula, S., Feng, H., Sellamuthu, R., Wu, T., MacVittie, T.J., and Orschell, C.M. (2019). Lifelong residual bone marrow damage in murine survivors of the hematopoietic acute radiation syndrome (H-ARS): a

compilation of studies comprising the Indiana University experience. Health Phys. *116*, 546–557.

Dainiak, N., Waselenko, J.K., Armitage, J.O., MacVittie, T.J., and Farese, A.M. (2003). The hematologist and radiation casualties. Hematol. Am. Soc. Hematol. Educ. Program, 473–496.

Dyson, H.J., and Wright, P.E. (2016). Role of intrinsic protein disorder in the function and interactions of the transcriptional coactivators CREB-binding protein (CBP) and p300. J. Biol. Chem. *291*, 6714–6722.

Faustman, D.L., and Davis, M. (2013). TNF receptor 2 and disease: autoimmunity and regenerative medicine. Front. Immunol. *4*, 478.

Fei, P., Bernhard, E.J., and El-Deiry, W.S. (2002). Tissue-specific induction of p53 targets in vivo. Cancer Res. *62*, 7316–7327.

Fischer, R., Maier, O., Siegemund, M., Wajant, H., Scheurich, P., and Pfizenmaier, K. (2011). A TNF receptor 2 selective agonist rescues human neurons from oxidative stress-induced cell death. PLoS One *6*, e27621.

Fleming, W.H., Alpern, E.J., Uchida, N., Ikuta, K., Spangrude, G.J., and Weissman, I.L. (1993). Functional heterogeneity is associated with the cell cycle status of murine hematopoietic stem cells. J. Cell Biol. *122*, 897–902.

Fujino, H., Salvi, S., and Regan, J.W. (2005). Differential regulation of phosphorylation of the cAMP response element-binding protein after activation of EP2 and EP4 prostanoid receptors by prostaglandin E2. Mol. Pharmacol. *68*, 251–259.

Gazit, R., Mandal, P.K., Ebina, W., Ben-Zvi, A., Nombela-Arrieta, C., Silberstein, L.E., and Rossi, D.J. (2014). Fgd5 identifies hematopoietic stem cells in the murine bone marrow. J. Exp. Med. *211*, 1315–1331.

Gentile, P., Byer, D., and Pelus, L.M. (1983). In vivo modulation of murine myelopoiesis following intravenous administration of prostaglandin E2. Blood *62*, 1100–1107.

Gentile, P.S., and Pelus, L.M. (1987). In vivo modulation of myelopoiesis by prostaglandin E2. II. Inhibition of granulocyte-monocyte progenitor cell (CFU-GM) cell-cycle rate. Exp. Hematol. *15*, 119–126.

Georgakilas, A.G., Bennett, P.V., Wilson, D.M., III, and Sutherland, B.M. (2004). Processing of bistranded abasic DNA clusters in gamma-irradiated human hematopoietic cells. Nucleic Acids Res. *32*, 5609–5620.

Hanson, W.R., and Ainsworth, E.J. (1985). 16,16-Dimethyl prostaglandin E2 induces radioprotection in murine intestinal and hematopoietic stem cells. Radiat. Res. *103*, 196–203.

Hanson, W.R., and Thomas, C. (1983). 16, 16-dimethyl prostaglandin E2 increases survival of murine intestinal stem cells when given before photon radiation. Radiat. Res. *96*, 393–398.

Hanson, W.R., Pelka, A.E., Nelson, A.K., and Malkinson, F.D. (1992). Subcutaneous or topical administration of 16,16 dimethyl prostaglandin E2 protects from radiation-induced alopecia in mice. Int. J. Radiat. Oncol. Biol. Phys. *23*, 333–337.

Hao, S., Chen, C., and Cheng, T. (2016). Cell cycle regulation of hematopoietic stem or progenitor cells. Int. J. Hematol. *103*, 487–497.

Himburg, H.A., Doan, P.L., Quarmyne, M., Yan, X., Sasine, J., Zhao, L., Hancock, G.V., Kan, J., Pohl, K.A., Tran, E., et al. (2017). Dickkopf-1 promotes hematopoietic regeneration via direct and niche-mediated mechanisms. Nat. Med. *23*, 91–99.

Hoggatt, J., and Pelus, L.M. (2010). Eicosanoid regulation of hematopoiesis and hematopoietic stem and progenitor trafficking. Leukemia *24*, 1993–2002.

Hoggatt, J., Singh, P., Sampath, J., and Pelus, L.M. (2009). Prostaglandin E2 enhances hematopoietic stem cell homing, survival, and proliferation. Blood *113*, 5444–5455.

Hoggatt, J., Mohammad, K.S., Singh, P., Hoggatt, A.F., Chitteti, B.R., Speth, J.M., Hu, P., Poteat, B.A., Stilger, K.N., Ferraro, F., et al. (2013a). Differential stem- and progenitor-cell trafficking by prostaglandin E2. Nature *495*, 365–369.

Hoggatt, J., Singh, P., Stilger, K.N., Plett, P.A., Sampson, C.H., Chua, H.L., Orschell, C.M., and Pelus, L.M. (2013b). Recovery from hematopoietic injury by modulating prostaglandin E(2) signaling post-irradiation. Blood Cells Mol. Dis. *50*, 147–153.

Insinga, A., Cicalese, A., Faretta, M., Gallo, B., Albano, L., Ronzoni, S., Furia, L., Viale, A., and Pelicci, P.G. (2013). DNA damage in stem cells activates p21, inhibits p53, and induces symmetric self-renewing divisions. Proc. Natl. Acad. Sci. U S A *110*, 3931–3936.

Kiel, M.J., Yilmaz, O.H., Iwashita, T., Yilmaz, O.H., Terhorst, C., and Morrison, S.J. (2005). SLAM family receptors distinguish hematopoietic stem and progenitor cells and reveal endothelial niches for stem cells. Cell *121*, 1109–1121.

Lee, C.L., Castle, K.D., Moding, E.J., Blum, J.M., Williams, N., Luo, L., Ma, Y., Borst, L.B., Kim, Y., and Kirsch, D.G. (2015). Acute DNA damage activates the tumour suppressor p53 to promote radiation-induced lymphoma. Nat. Commun. *6*, 8477.

Liu, Y., Elf, S.E., Miyata, Y., Sashida, G., Liu, Y., Huang, G., Di, G.S., Lee, J.M., Deblasio, A., Menendez, S., et al. (2009). p53 regulates hematopoietic stem cell quiescence. Cell Stem Cell *4*, 37–48.

Ludin, A., Gur-Cohen, S., Golan, K., Kaufmann, K.B., Itkin, T., Medaglia, C., Lu, X.J., Ledergor, G., Kollet, O., and Lapidot, T. (2014). Reactive oxygen species regulate hematopoietic stem cell self-renewal, migration and development, as well as their bone marrow microenvironment. Antioxid. Redox Signal. *21*, 1605–1619.

Maier, O., Fischer, R., Agresti, C., and Pfizenmaier, K. (2013). TNF receptor 2 protects oligodendrocyte progenitor cells against oxidative stress. Biochem. Biophys. Res. Commun. *440*, 336–341.

Mariotti, L.G., Pirovano, G., Savage, K.I., Ghita, M., Ottolenghi, A., Prise, K.M., and Schettino, G. (2013). Use of the gamma-H2AX assay to investigate DNA repair dynamics following multiple radiation exposures. PLoS One *8*, e79541.

Mayr, B., and Montminy, M. (2001). Transcriptional regulation by the phosphorylation-dependent factor CREB. Nat. Rev. Mol. Cell Biol. *2*, 599–609.

Mohrin, M., Bourke, E., Alexander, D., Warr, M.R., Barry-Holson, K., Le Beau, M.M., Morrison, C.G., and Passegue, E. (2010). Hematopoietic stem cell quiescence promotes error-prone DNA repair and mutagenesis. Cell Stem Cell *7*, 174–185.

Muller, M., Wilder, S., Bannasch, D., Israeli, D., Lehlbach, K., Li-Weber, M., Friedman, S.L., Galle, P.R., Stremmel, W., Oren, M.,

and Krammer, P.H. (1998). p53 activates the CD95 (APO-1/Fas) gene in response to DNA damage by anticancer drugs. J. Exp. Med. *188*, 2033–2045.

Naude, P.J., den Boer, J.A., Luiten, P.G., and Eisel, U.L. (2011). Tumor necrosis factor receptor cross-talk. FEBS J. *278*, 888–898.

North, T.E., Goessling, W., Walkley, C.R., Lengerke, C., Kopani, K.R., Lord, A.M., Weber, G.J., Bowman, T.V., Jang, I.H., Grosser, T., et al. (2007). Prostaglandin E2 regulates vertebrate haematopoietic stem cell homeostasis. Nature *447*, 1007–1011.

Oguro, H., Ding, L., and Morrison, S.J. (2013). SLAM family markers resolve functionally distinct subpopulations of hematopoietic stem cells and multipotent progenitors. Cell Stem Cell *13*, 102–116.

Parry, G.C., and Mackman, N. (1997). Role of cyclic AMP response element-binding protein in cyclic AMP inhibition of NF-kappaB-mediated transcription. J. Immunol. *159*, 5450–5456.

Passegue, E., Wagers, A.J., Giuriato, S., Anderson, W.C., and Weissman, I.L. (2005). Global analysis of proliferation and cell cycle gene expression in the regulation of hematopoietic stem and progenitor cell fates. J. Exp. Med. *202*, 1599–1611.

Pawlik, A., Alibert, O., Baulande, S., Vaigot, P., and Tronik-Le, R.D. (2011). Transcriptome characterization uncovers the molecular response of hematopoietic cells to ionizing radiation. Radiat. Res. *175*, 66–82.

Pelus, L.M. (1982). Association between colony forming units-granulocyte macrophage expression of Ia-like (HLA-DR) antigen and control of granulocyte and macrophage production. A new role for prostaglandin E. J. Clin. Invest. *70*, 568–578.

Pelus, L.M., and Hoggatt, J. (2011). Pleiotropic effects of prostaglandin E2 in hematopoiesis; prostaglandin E2 and other eicosanoids regulate hematopoietic stem and progenitor cell function. Prostaglandins Other Lipid Mediat. *96*, 3–9.

Plett, P.A., Sampson, C.H., Chua, H.L., Joshi, M., Booth, C., Gough, A., Johnson, C.S., Katz, B.P., Farese, A.M., Parker, J., et al. (2012). Establishing a murine model of the hematopoietic syndrome of the acute radiation syndrome. Health Phys. *103*, 343–355.

Porter, R.L., Georger, M.A., Bromberg, O., McGrath, K.E., Frisch, B.J., Becker, M.W., and Calvi, L.M. (2013). Prostaglandin E2 increases hematopoietic stem cell survival and accelerates hematopoietic recovery after radiation injury. Stem Cells *31*, 372–383.

Sage, E., and Shikazono, N. (2017). Radiation-induced clustered DNA lesions: repair and mutagenesis. Free Radic. Biol. Med. *107*, 125–135.

Seita, J., and Weissman, I.L. (2010). Hematopoietic stem cell: self-renewal versus differentiation. Wiley. Interdiscip. Rev. Syst. Biol. Med. *2*, 640–653.

Shao, L., Luo, Y., and Zhou, D. (2014). Hematopoietic stem cell injury induced by ionizing radiation. Antioxid. Redox Signal. *20*, 1447–1462.

Simonnet, A.J., Nehme, J., Vaigot, P., Barroca, V., Leboulch, P., and Tronik-Le, R.D. (2009). Phenotypic and functional changes induced in hematopoietic stem/progenitor cells after gamma-ray radiation exposure. Stem Cells *27*, 1400–1409.

St-Pierre, J., Drori, S., Uldry, M., Silvaggi, J.M., Rhee, J., Jager, S., Handschin, C., Zheng, K., Lin, J., Yang, W., et al. (2006). Suppression of reactive oxygen species and neurodegeneration by the PGC-1 transcriptional coactivators. Cell *127*, 397–408.

Staszewski, O., Nikolova, T., and Kaina, B. (2008). Kinetics of gamma-H2AX focus formation upon treatment of cells with UV light and alkylating agents. Environ. Mol. Mutagen. *49*, 734–740.

Steel, L.K., Walden, T.L., Jr., Hughes, H.N., and Jackson, W.E., III. (1988). Protection of mice against mixed fission neutron-gamma (n:gamma = 1:1) irradiation by WR-2721, 16,16-dimethyl PGE2, and the combination of both agents. Radiat. Res. *115*, 605–608.

Till, J.E., and McCulloch, E.A. (1964). Repair processes in irradiated mouse hematopoieetic tissue. Ann. N. Y. Acad. Sci. *114*, 115–125.

van Buul, P.P., van Duyn-Goedhart, A., and Sankaranarayanan, K. (1999). In vivo and in vitro radioprotective effects of the prostaglandin E1 analogue misoprostol in DNA repair-proficient and -deficient rodent cell systems. Radiat. Res. *152*, 398–403.

Walden, T.L., Jr., Patchen, M., and Snyder, S.L. (1987). 16,16-Dimethyl prostaglandin E2 increases survival in mice following irradiation. Radiat. Res. *109*, 440–448.

Yamashita, M., and Passegue, E. (2019). TNF-alpha coordinates hematopoietic stem cell survival and myeloid regeneration. Cell Stem Cell *25*, 357–372.

Yu, H., Shen, H., Yuan, Y., XuFeng, R., Hu, X., Garrison, S.P., Zhang, L., Yu, J., Zambetti, G.P., and Cheng, T. (2010). Deletion of Puma protects hematopoietic stem cells and confers long-term survival in response to high-dose gamma-irradiation. Blood *115*, 3472–3480.